Korean J. Chem. Eng., 34(7), 1952-1960 (2017)
DOI: 10.1007/s11814-017-0117-y

pISSN: 0256-1115
eISSN: 1975-7220

A comparative study of models for molten carbonate fuel cell (MCFC) processes

Tae Young Kim, Beom Seok Kim, Tae Chang Park, and Yeong Koo Yeo†

Department of Chemical Engineering, Hanyang University, Seoul 04763, Korea
(*Received 11 December 2016 • accepted 22 April 2017*)

Abstract−The necessity of this work arose from the need for identification of a comprehensive plant model that can be used in the model-based control of the MCFC plant. Various models for molten carbonate fuel cell (MCFC) processes are presented and evaluated in this paper. Both a rigorous model based on mass and energy balances and implicit models based on operation data were investigated and analyzed. In particular, auto-regressive moving average (ARMA) model, least-squares support vector machine (LSSVM) model, artificial neural network (ANN) model and partial least squares (PLS) model for a MCFC system were developed based on input-output operating data. Among these models, the ARMA model showed the best agreement with plant operation data.

Keywords: Molten Carbonate Fuel Cell, ARMA Modeling, Partial Least Squares, Artificial Neural Network, Least-squares Support Vector Machine

INTRODUCTION

A molten carbon fuel cell (MCFC) is well known to be an efficient clean energy generating facility. Among various types of fuel cell technologies, the MCFC is one of the readily available devices that are available in MW scale. A typical MCFC plant utilizes internal reforming of natural gas, and it is not necessary to use a large external reformer to generate hydrogen fuel, resulting in the simple and compact plant configuration. In a typical MCFC system, chemical energy contained in fuel and oxidizer is converted to electric energy via electrochemical reaction. It is well known that MCFC is one of the most efficient technologies to replace the fossil fuel burning thermal power plants which induce significant pollution emission. MCFC has evolved as a new generation of power source, and relevant technology has been developed in large scale by many countries, including the United States, Europe, Japan and Korea. So far, modeling of MCFC processes has been focused on such issues as physical, chemical and transport properties, reaction kinetics, and static operation performance. From the operational point of view, simple expressions of fuel cells and balance-of-plant (BOP) are preferred for use in model-based control applications. Recently, several developments in the modeling of MCFC based on balance equations and specific assumptions have been reported. Effects of fuel cell geometry and complicated mass distributions on the plant performance were taken into account in a rigorous model for external reforming MCFC systems [1,2]. A rigorous model for internal reforming MCFC reported is based on the assumptions of equilibrium chemical reactions and negligible mass accumulation [3]. A lumped-parameter model was developed based on the expression of dynamics using mass storage, polarization losses and kinetics of reforming reactions [4]. Most of the existing rigorous models developed so far are based on mass, energy and momentum conservation laws, and their expression are too complicated to be used to design a model based control system. The applicability of the rigorous model to a controller is usually restricted to adjustment of operation conditions. Li [5] proposed dynamic modeling and control of crude terephthalic acid hydropurification process. Sheng [6] proposed a control strategy based on the steady-state optimization involving two PID controllers. Many algorithms for modeling and control based on artificial neural networks have been presented [7]. Shen et al. [8] presented an adaptive fuzzy control scheme for the temperature control of MCFC stack using a neural network identification model. Faisal Ahmed [9] presented a prediction of NOx emission from coal-fired power plant using a least-squares supporting vector machine. In this work, an auto-regressive moving average (ARMA) model, a least-squares supporting vector machine (LSSVM), an artificial neural network (ANN) model and a partial least squares (PLS) as well as the rigorous model are proposed to describe the MCFC plant which is being operated with capacity of 2.5 MW. These models can be effectively used to analyze and to estimate dynamic behavior of underlying MCFC plant. The tracking performance of these models was investigated and compared with each other based on operating data. For the purpose of control, it turned out that the ARMA model can be effectively used since it is more compact and simpler than other models.

PROCESS DESCRIPTION

Fig. 1 shows the basic layout of the MCFC system. Mechanical balance of plant is a mechanical device of control and operating fuel cell stack. Water is normally taken directly from the local municipal supply and then flows through a water purifier. Some of the water must be discharged to drain as part of the water purification processes, although in some projects this water can be reclaimed or collected for auxiliary purposes.

Fuel gas is a mixture of steam and methane that is fed into the

†To whom correspondence should be addressed.
E-mail: ykyeo@hanyang.ac.kr

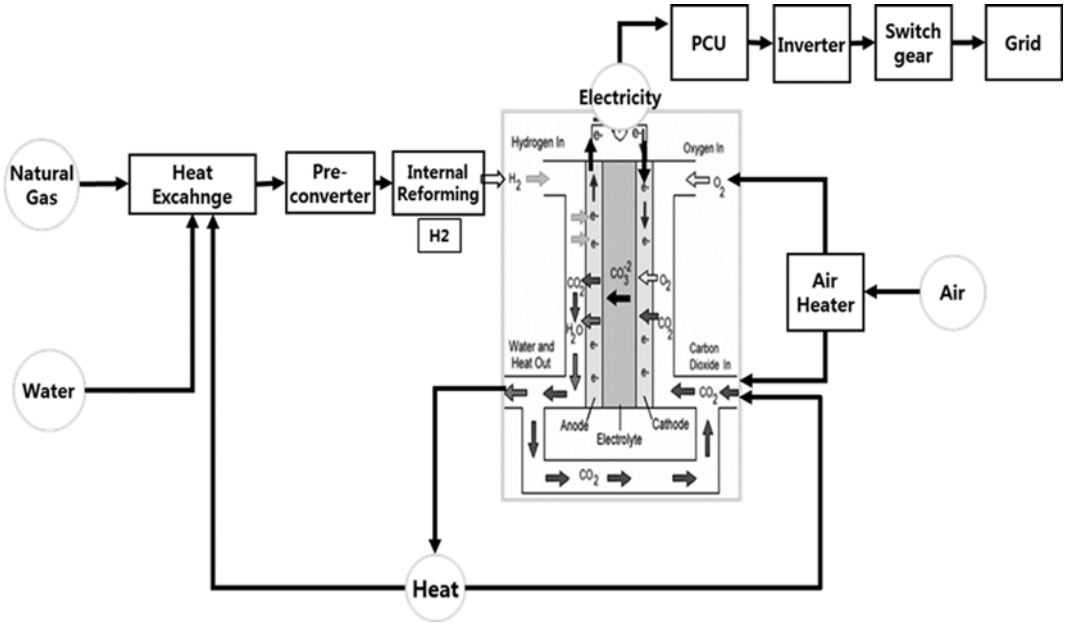

Fig. 1. Layout of the MCFC system.

stack's reforming units and anodes. Natural gas flows through desulfurizers to remove sulfur compounds. If allowed to break through, these sulfur compounds would damage the catalysts in the stack and pre-converter. The majority of the desulfurized natural gas is delivered to the humidifier where it is mixed with the purified water and heated using cathode exhaust gases to form fuel gas. The remainder of the natural gas is provided to the air heater. The fuel gas then passes through a vessel called the deoxidizer and the pre-converter which contains two types of catalyst. The first catalyst is the deoxidizer catalyst used to remove oxygen from the fuel gas by reacting it with the methane.

MODELING OF MCFC PROCESS

1. Rigorous Model

In a typical MCFC process, natural gas is reformed to hydrogen in the internal reforming unit and the cells. Fig. 2 shows the two-step approach consisting of indirect and direct internal reforming (IIR and DIR) [10]. In the IIR step, a reforming unit is placed between every ten fuel cell units in the stack and converts about 50% of natural gas to hydrogen prior to entering into the cell anode. Further reforming occurs in the cell anodes (DIR step) that are loaded with reforming catalysts. The following electrochemical reactions are considered to be taking place in the underlying MCFC plant. We can see that additional fuel (i.e., H_2) is produced in the water-gas shift reaction.

$$\text{Cathode: } CO_2 + \frac{1}{2}O_2 + 2e^- \rightarrow CO_2^{-2} \quad (1)$$

$$\text{Anode: } H_2 + CO_2^{-2} + 2e^- \rightarrow H_2O + CO_2 + 2e^- \quad (2)$$

$$\text{Total: } H_2 + O_2 \rightarrow \text{Electricity} + \text{Heat} \quad (3)$$

Both of the following independent reactions occur in the IIR and the DIR step simultaneously:

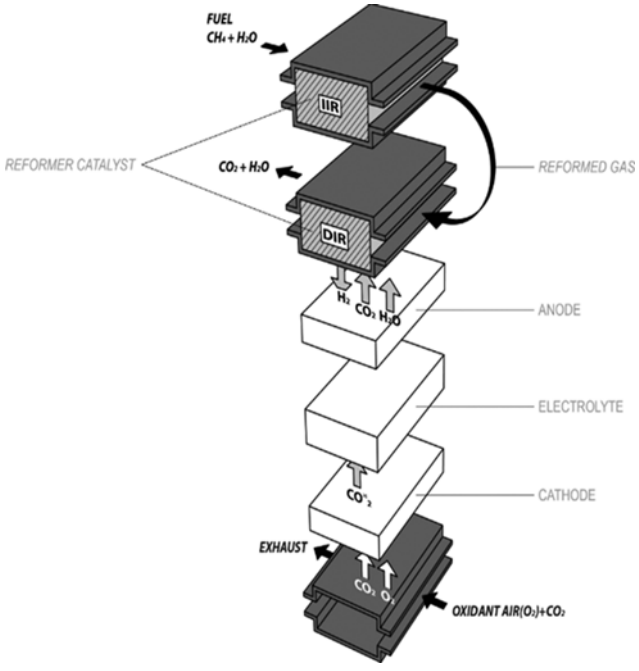

Fig. 2. IIR/DIR structure of MCFC stack.

$$\text{Reforming: } CH_4 + H_2O \rightarrow CO + 3H_2 \quad (4)$$

$$\text{Water-gas shift: } CO + H_2O \leftrightarrow CO_2 + H_2 \quad (5)$$

Actual performance (voltage) of the fuel cell for a specified load current is dependent upon the chemical reactants and products as well as the cell temperature. Since each stack operates under the same operating conditions, the rigorous model considers a lumped

expression of all equivalent stacks. The reforming unit and the anode compartments are lumped together and are referred to as the anode hereafter. Anode and cathode are usually considered as two well-stirred compartments with mass (ions) interchange through the electrolyte matrix separating the two compartments.

Temperatures of anode and cathode are nearly equal to each other, and elementary mole balances for each anode and cathode compartment can be represented as follows [11]:

$$V\tilde{C}_t\frac{dx_i}{dt}=N^{in}(x_i^{in}-x_i)-x_i\sum_{i=1}^{\xi}R_i+R_i,\ \ i=1,\ \ldots,\ \xi \tag{6}$$

where V is the volume of the compartment (m^3), $\tilde{C}_t$ is the total molar concentration (mol/m^3), N^{in} is the total molar flow into V (mol/s), x_i^{in} is the inlet mole fraction of component i, x_i denotes the mole fraction of component i, and ξ is the number of different species. R_i represents the rate of production of species i.

$$R_i=\sum v_{ij}r_i \tag{7}$$

where v_{ij} are the stoichiometric coefficients of species i in the reaction j (in the reforming reaction (4), H_2 has a coefficient 3), and r_i is the molar extent of reaction in the reaction j.

Pressure dynamics at anode and cathode can be obtained by differentiating the equation of the ideal gas law with respect to time [12,13]. Mass balances in the anode and cathode can be given by

$$\frac{P_{an}V_{an}}{RT}\frac{dx_i}{dt}=N_{an}^{in}x_i^{in}-N_{an}^{out}x_i^{out}+\sum v_{ij}r_i$$
$$i_{anode}\in\{H_2,\ H_2O,\ CH_4,\ CO,\ CO_2,\ N_2\} \tag{8}$$

$$\frac{P_{ca}V_{ca}}{RT}\frac{dx_i}{dt}=N_{ca}^{in}x_i^{in}-N_{ca}^{out}x_i^{out}+\sum v_{ij}r_i$$
$$i_{cathods}\in\{H_2O,\ CO_2,\ O_2,\ N_2\} \tag{9}$$

The reaction rate in the cell follows the Faraday's law:

$$r_e=\frac{AJ}{2F} \tag{10}$$

where A is the cell area (cm^2), J is the current density (J/kg/K), and F is the Faraday coefficient (J/mol/V). The reaction rate in the reformer can be represented as follows [14]:

$$\text{Reforming: } r_s=Ak_sp_{CH_4}\exp\left(-\frac{E_A}{RT}\right),\ E_A=82\ \text{kJ/mol} \tag{11}$$

$$\text{WGS: } r_w=Ak_w\left(1-\frac{p_{H_2}p_{CO}}{p_{H_2O}p_{CO}K_w}\right),\ K_W=\exp\left(\frac{4276}{T}-33.961\right) \tag{12}$$

where k_s and k_w are the rate constants for each reaction, E_A is the activation energy and K_W represents the equilibrium constant. Electrical performance of the fuel cell can be expressed in terms of temperature and gas compositions by the Nernst equation [15]:

$$V_0=E_0(T)+\frac{RT}{2F}\ln\frac{P_{H_2,a}P_{O_2}^{1/2},\ c,\ P_{CO^2,c}}{P_{H_2O,a}P_{CO,a}} \tag{13}$$

where V_0 is the equilibrium potential, $E_0(T)$ represents the cell standard potential, and P_i denotes the partial pressure of gas species i. The actual cell voltage is represented by the equilibrium cell potential and irreversible losses. The irreversible losses in the fuel cell are contributed by activation, concentration, and ohmic polarizations:

$$V_{cell}=V_0-\eta_{act}-\eta_{conc}-iz \tag{14}$$

where V_{cell} is the cell voltage under load (V), η_{act} denotes the activation polarization (V), η_{conc} represents the concentration polarization (V), and z is the cell ohmic impedance ($\Omega\ cm^2$). Dynamics of the stack temperature can be represented by the following energy balance equation:

$$m_s\overline{C}_{ps}\frac{dT_s}{dt}=\sum\dot{n}_i^{in}\int_{T_{ref}}^{T_{in}}C_{p,i}(T)dT$$
$$-\sum\dot{n}_i^{out}\int_{T_{ref}}^{T_s}C_{p,i}(T)dT-\dot{n}_{H_2}^{r}\Delta\hat{H}_r^o-V_{cell}I \tag{15}$$

where m_s and $\overline{C}_{ps}$ represent the mass and average specific heats of cell materials, respectively, $C_{p,i}$ is the specific heat of i^{th} fuel or air entering the system, $\Delta\hat{H}_r^o$ is the specific heat of total reaction (3).

Fuel utilization is defined as the fraction of total fuel introduced into the cell that is consumed by electrochemical reactions:

$$U_f\equiv\frac{H_{2,\ consumed}}{H_{2,\ in}} \tag{16}$$

where $H_{2,consumed}$ is the rate of consumption of hydrogen in the electrochemical reaction and $H_{2,in}$ is the molar flowrate of hydrogen into the fuel cell. For the internal reforming MCFC, $H_{2,in}$ is defined to account for internal generation of hydrogen:

$$H_{2,\ in}\equiv N_{ru}^{in}(x_{ru,\ H_2}^{in}+4x_{ru,\ CH_4}^{in}+x_{ru,\ CO}^{in}) \tag{17}$$

where N_{ru}^{in} is the total inlet molar flow to the reforming unit, and the $x_{ru,\ i}^{in}$ represents the mole fraction of the reforming unit inlet gas. This equation represents H_2 generated by: (1) upstream reaction (pre-converter); (2) reforming reaction (reforming unit and cell); and (3) water-gas shift reaction (reforming unit and cell). The coefficient U_f in Eq. (16) follows from reactions (3) and (4). Faraday's law (9) can be used to replace $H_{2,consumed}$ by using the system DC current I_{sys} in the expression for fuel utilization. It is supposed that there are 4 model (258 cell per module) in the 2.5 MW MCFC plant being considered in this work:

$$U_f=\frac{C_{total}I_{sys}}{2FH_{2,\ in}},\ C_{total}=4*258 \tag{18}$$

Steam-carbon ratio is simply defined as the molar ratio of steam to methane:

$$\text{s/c ratio}\equiv\frac{x_{H_2O}}{x_{CH_4}}=\frac{N_{H_2O}}{N_{CH_4}} \tag{19}$$

Fig. 3 shows results of numerical estimations for target variables (voltage (a), fuel utilization (b) and steam to carbon ratio (c)) based on the rigorous model. The voltage calculated by the rigorous model is displayed as well as operation data when the current density increases from 118 mA/cm^2 to 130 mA/cm^2. The power (voltage) tends to decrease because the voltage is inversely proportional to the current density. From Fig. 3, we can see that discrepancy between the simulation results and operation data increases over time.

2. Auto-regressive Moving Average (ARMA) Model

ARMA model is adequate to interpret statistical time-series data and to estimate output values. In an auto-regression model, a linear combination of past data is used to estimate the variable of inter-

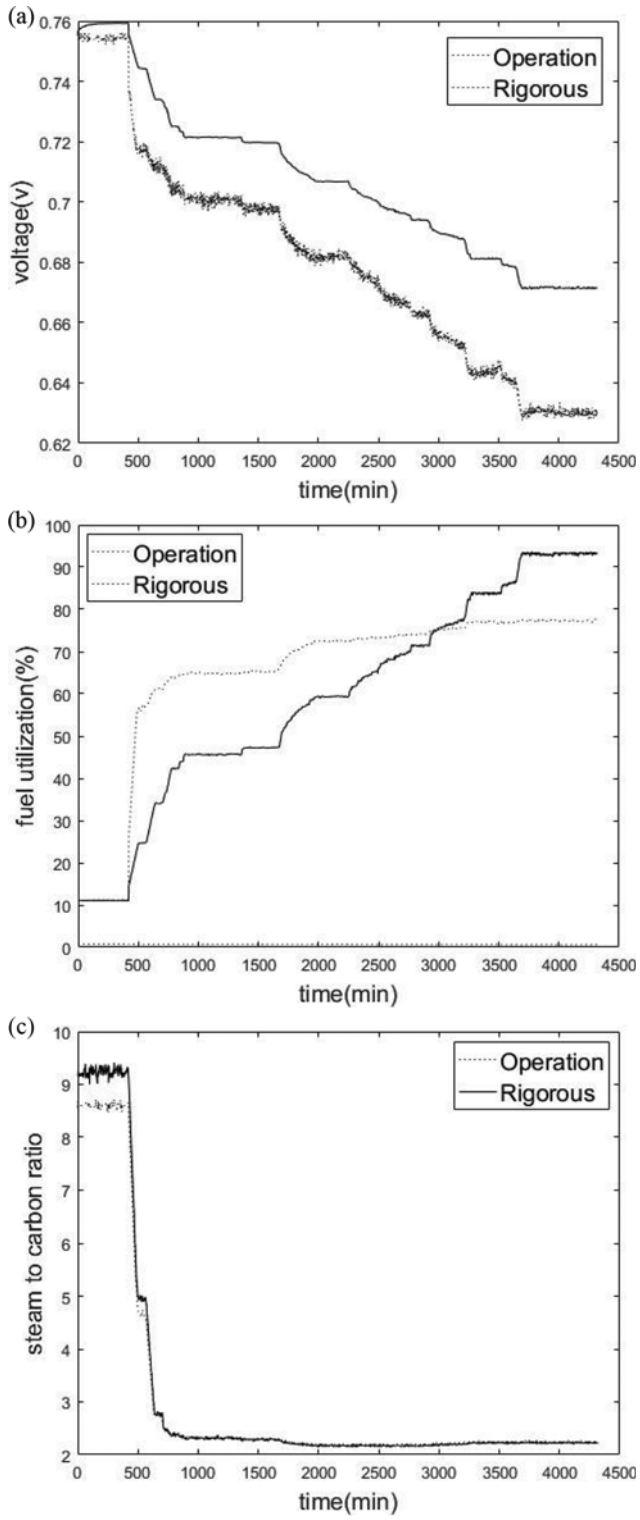

Fig. 3. Simulation results by using a rigorous model: (a) Voltage, (b) fuel utilization and (c) steam to carbon ratio.

est. An auto-regressive model of order p can be expressed as

$$X_t = \emptyset_1 X_{t-1} + \emptyset_2 X_{t-2} \ldots + \emptyset_p X_{t-p} + V_t \quad (20)$$

where V_t represents modeling error. This is a multiple regression with lagged values of X_t being used as predictors. This model is also referred to as an AR(p) model. It is well known that auto-regressive models are very efficient at treating a wide range of various time-series patterns. A moving average model employs past estimation errors instead of using past values of the forecast variables:

$$V_t = w_t + \theta_1 w_{t-1} + \theta_2 w_{t-2} \ldots + \theta_q w_{t-q} \quad (21)$$

where w_t represents white noise.

This model is referred to as an MA(q) model. In the AR model, X_t may be regarded as a weighted moving-average of some of the past estimation errors. Combination of these two equations gives the model for X_t represented by ARMA (p, q). In this expression, p represents the auto-regressive part order, which is the order of the moving average part. It can be seen that the ARMA model is static if the model is expressed as [16]:

$$X_t - \emptyset_1 X_{t-1} - \cdots - \emptyset_p X_{t-p} = w_t + \theta_1 w_{t-1} + \cdots + \theta_q w_{t-q} \; w_t \sim WN(0, \sigma^2) \quad (22)$$

We can abbreviate Eq. (22) using the so-called backshift operator defined as $B^k X_t = X_{t-k}$. Using the B operator, Eq. (22) can be written as

$$\emptyset(z) X_t = q(z) w_t \quad (23)$$

where

$$\emptyset(z) = 1 - \emptyset_1 z - \cdots - \emptyset_p z^p, \; \theta(z) = 1 + \theta_1 z + \cdots + \theta_q z^q$$

The data for the air, water and natural gas flow rates in time are used to estimate values of coefficients in Eq. (23). The hydrogen flow involved in the reaction is used directly instead of the natural gas flow in the modeling of the MCFC plant. The air, hydrogen and water flow rates are taken as manipulated variables (u_1, u_2, u_3), and the power, fuel utilization and s/c ratio are regarded as controlled target variables to give the desired linear relation. The coefficients were estimated based on the operating data of the 2.5 MW MCFC plant being operated in Kyungki-Do, Korea. Table 1 shows coefficients of the ARMA model obtained for various target variables.

Table 1. Coefficients of the ARMA model for various target variables

Target variable	Manipulated variable			
	Air flow (u_1)	Hydrogen flow (u_2)	Water flow (u_3)	Constant
Voltage	−0.2499	−0.9907	0.4128	0.8423
Fuel utilization	0.1681	0.7882	−0.6340	0.3386
Steam-carbon ratio	−0.1019	0.6961	1.0558	0.3979

Fig. 4 shows results of numerical estimations for target variables (voltage (a), fuel utilization (b) and steam to carbon ratio (c)) based on the ARMA model. We can see that the proposed ARMA model shows much better tracking performance for target variable.

3. Least-squares Support Vector Machine (LSSVM) Model

SVM was first introduced for classification of data and estimation of nonlinear function, and further investigated by many investigators [17]. The SVM for regression is formulated in resolving optimization problems involving a quadratic programming (QP) problem. However, the large computational burden involved in the

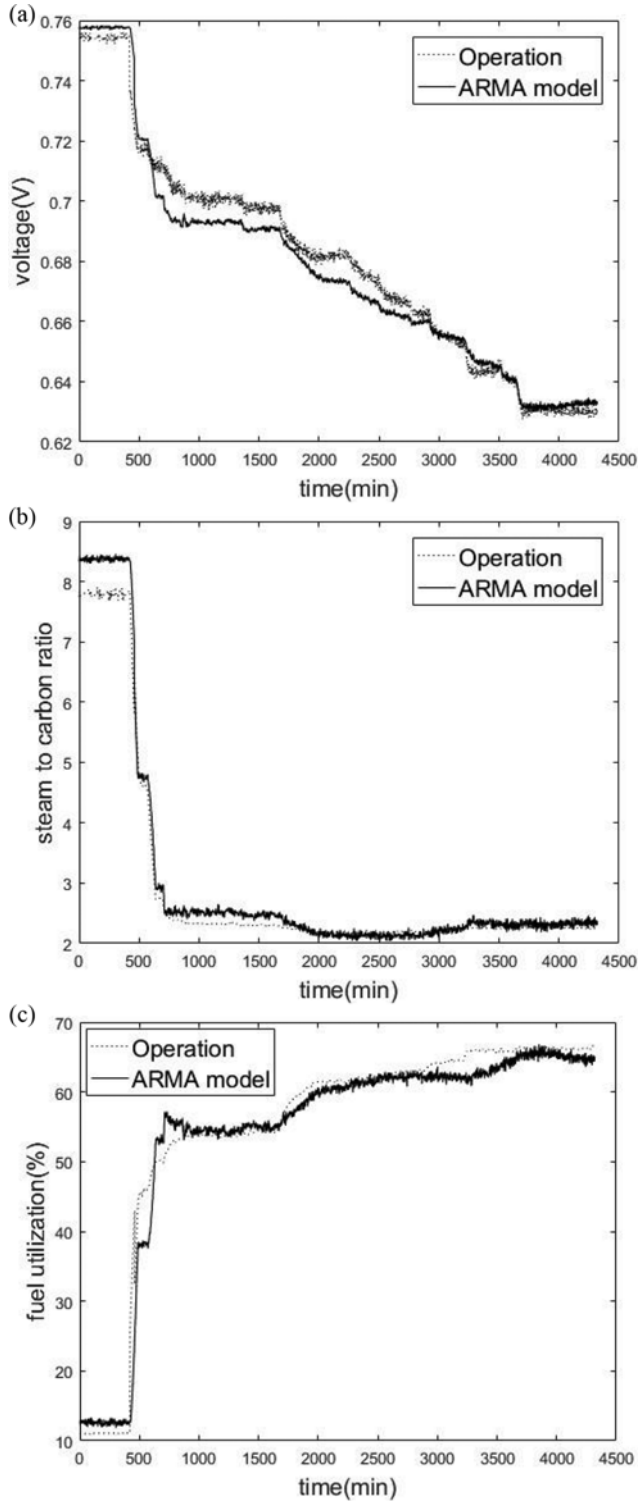

Fig. 4. Simulation results by using ARMA model: (a) Voltage, (b) fuel utilization and (c) steam to carbon ratio.

solution of the constrained optimization programming problem may be considered as the major drawback of SVM. Major breakthrough has been obtained with a least squares version of SVM, called LSSVM. In LSSVM [18,19], as in the training of artificial neural networks, a cost function consisting of a sum of squared error (SSE) and equality constraints is used. By doing this, the problem may be greatly simplified, and numerical techniques employed to handle linear systems can be used efficiently. In fact, iterative methods such as the conjugate gradient scheme can be used to solve the corresponding linear systems.

Consider a training set consisting of N data points $\{x_k, y_k\}_{k=1}^N$ with input data $x_k \in \mathbf{R}^N$ and output $y_k \in r$ where $\mathbf{R}^N$ is the N-dimensional vector and r denotes an one-dimensional vector. The three input variables used for the LSSVM model in this study are air flow (AF), hydrogen flow (HF), and water flow (WF): x=[AF, HF, WF]. The output (y) in the LS-SVM model is target variable (V_t) which may be voltage, fuel utilization or steam to carbon ratio: $y=V_t$.

In feature space LSSVM models take the form

$$y(x)=\omega^T\varphi(x)+b \tag{24}$$

where ω represents an adjustable weight vector and $b \in r$ is the scalar threshold. The nonlinear mapping denoted by $\varphi(.)$ maps the input data to a feature space $\omega \in \mathbf{R}^N$. In LSSVM intended for function estimation, a quadratic optimization problem is formulated as the following:

$$\text{Minimize: } 0.5\omega^T\omega+0.5\gamma\sum_{k=1}^{N}e_k^2$$

$$\text{Subject to: } y(x)=\omega^T\varphi(x_k)+b+e_k,\ k=1, \ldots, N \tag{25}$$

where e_k is the error variable and γ is a regularization parameter. Smaller γ can avoid overfitting in case of noisy data. Note that the cost function includes SSE, fitting error, and a term representing regularization, which is a standard strategy in the training of feedforward neural networks and is related to ridge regression.

The Lagrangian is given by

$$L_{LS\text{-}SVM}=\frac{1}{2}\|\omega\|^2+\gamma\frac{1}{2}\sum_{k=1}^{N}e_k^2-\sum_{k=1}^{N}\alpha_k\{\langle\omega,\ \varphi(x_k)\rangle+b+e_k-y_k\} \tag{26}$$

with Lagrange multipliers $\alpha_k \in R$. The optimality is given by

$$\begin{cases}\partial L_{LS\text{-}SVM}/\partial w=0\rightarrow\omega=\sum_{k=1}^{N}\alpha_k\varphi(x_k)\\ \partial L_{LS\text{-}SVM}/\partial b=0\rightarrow\sum_{k=1}^{N}\alpha_k=0\\ \partial L_{LS\text{-}SVM}/\partial e_k=0\rightarrow\alpha_k=\gamma e_k,\ (k=1, \ldots, N)\\ \partial L_{LS\text{-}SVM}/\partial\alpha_k=0\rightarrow\langle\omega,\ \varphi(x_k)\rangle+b+e_k-y_k=0\end{cases} \tag{27}$$

The conditions represented by (27) are similar to those of standard SVM optimality, except for $\alpha_k=\gamma e_k$, for which the sparseness property has been lost in LSSVM. After elimination of e_k, we obtain the following linear equations:

$$\begin{bmatrix}0 & 1_v^T\\ 1 & \Omega+I/\gamma\end{bmatrix}\begin{bmatrix}b\\ \alpha\end{bmatrix}=\begin{bmatrix}0\\ y\end{bmatrix} \tag{28}$$

where $y=[y_1; \ldots; y_N]$, $1_v=[1; \ldots; 1]$, $\alpha=[\alpha_1; \ldots; \alpha_N]$ and the Mercer condition has been applied again as shown below:

$$\Omega_{kl}=\langle\varphi(x_k),\ \varphi(x_l)\rangle=K(x_k, x_l)\ \ k, l=1, \ldots, N \tag{29}$$

Although the same kernel function K(·,·) used in SVM is employed in LSSVM, the powerful radial-basis function kernel is preferred. The LSSVM model for function estimation can be expressed as

$$VT = y(x) = \sum_{k=1}^{N} \alpha_k K(x, x_k) + b \quad (30)$$

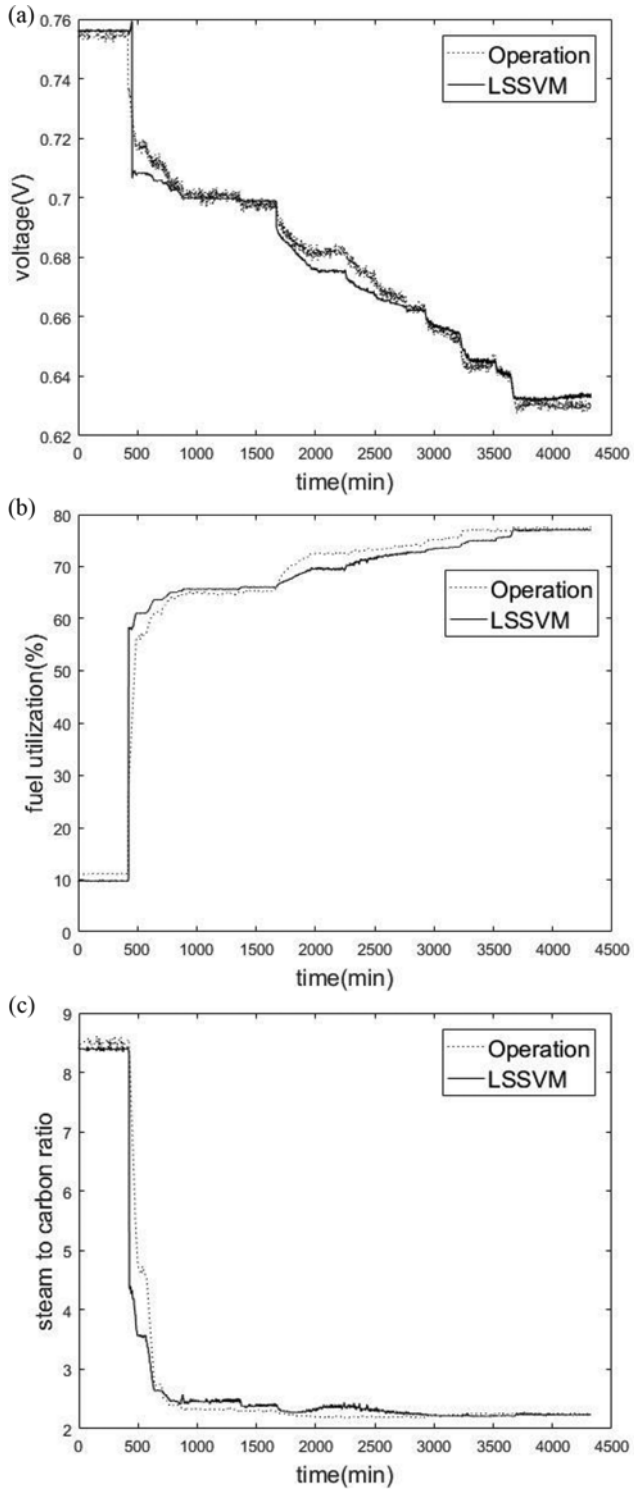

Fig. 5. Simulation results by using LS-SVM model: (a) Voltage, (b) fuel utilization and (c) steam to carbon ratio.

where α and b are the solutions to Eq. (28), respectively, and K(x, x_k) is the kernel function. The radial basis function being used as a kernel function in this analysis is given by

$$K(x_k, x_l) = \exp\{-(x_k - x_l)(x_k - x_k)^T / 2\sigma^2\}, \; k = \mathbf{1}, \ldots, N \quad (31)$$

where σ represents the width of the kernel function (radial basis function).

To be used in the derivation of LSSVM model for the underlying MCFC plant, the operation data are separated into two subsets: a training dataset to be used to construct the model, and a test dataset to validate the model performance. In this study, the training dataset consists of 8411 data points and the test dataset consists of 4,320 data points. Each data point has the unit of minute. The operation dataset consisting of 11,831 data points is divided into the training dataset and the test (i.e., validation) dataset. The training dataset, consisting of the first 8,411 data points of the operation dataset, was obtained during the commissioning period, and the test dataset consisting of remaining 4,320 data points was obtained during the reduced voltage operation period. The data are scaled between 0 and 1. The design values of the γ and σ are determined during the training of LSSVM. Fig. 5 shows estimation results of target variables (voltage (a), fuel utilization (b) and steam to carbon ratio (c)) obtained by using the LSSVM model. Comparison of Fig. 4 and 5 shows that both ARMA model and LSSVM model exhibit similar tracking performance.

4. Artificial Neural Network (ANN) Model

An important aspect of ANN is that it may highly approach a nonlinear mapping of two different dimensional spaces [20]. Theoretically, it was already proven that a tri-layer feed forward neural network can approximate any continuous functions by the free precision after training [21]. The sigmoid function is widely used for the actuating function of computation node of the network. In the ANN model, the input vector of the hidden layer $\{S_j\}$ is computed when the study sample $A_k=(a_1^k, a_2^k, \cdots, a_n^k)$ is fed into the input layer of the ANN model, and then the output vector of the hidden layer, $\{B_j\}$, is computed through the sigmoid function:

$$B_j = \sigma(S_j) = \sigma\left(\sum_{i=1}^{N} W_{ij} \cdot a_j - \theta_j\right) \quad (32)$$

where A_k is the input vector to the internal recurrent neural network (IRNN) model, W_{ij} is the connection weight of the input layer to the hidden layer and θ_j is the threshold of the output layer. Next, the input vector of the output layer $\{L_t\}$ is computed, and then the output vector of the output layer, $\{C_i^k\}$, is computed through the sigmoid function:

$$C_t^k = \sigma(L_t) = \sigma\left(\sum_{j=1}^{p} V_{jt} \cdot b_j - \gamma_t\right) \quad (33)$$

where γ_t is the threshold of the output layer and V_{jt} is the connection weight of the hidden layer to the output layer. The error of the network node is calculated backward according to the gradient drop law, and then the connection weights of the network are corrected through the backward propagation of the accumulated error. This procedure is repeated constantly until the pattern training of the k groups is completed. In the end, the overall root-

mean-square error of the whole network, E, is obtained as follows:

$$E = \sum_{k=1}^{m}\sum_{t=1}^{q}\sqrt{(y_t^k - C_t^k)^2} \quad (34)$$

where Y_k is the expected output vector of the ANN model. Finally, the output vector of the ANN with the bias node is given by:

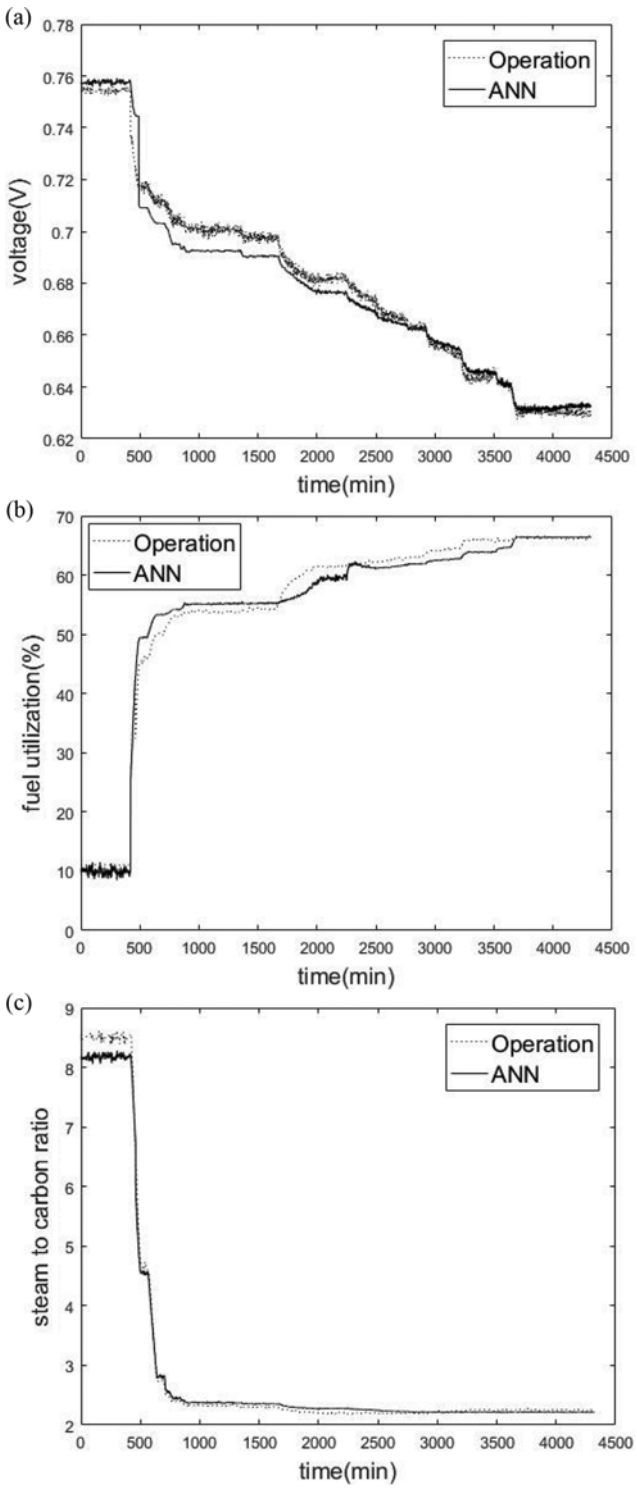

Fig. 6. Simulation results by using ANN model: (a) Voltage, (b) fuel utilization and (c) steam to carbon ratio.

$$Y(k) = \sum_{j=1}^{p} WO_j \cdot \sigma(S_j(k)) + WO_{bias} \quad (35)$$

$$S_j(k) = \sum_{i=1}^{p} WR_{ij} \cdot \sigma(S_j(k-1)) + \sum_{i=1}^{n} WI_{ij} \cdot I_i(k) + WI_{jbias} \quad (36)$$

where WI, WR and WO are the weight coefficients from the input layer to the hidden layer, from the feedback layer to the hidden layer, and from the hidden layer to the output layer, respectively, I is the input vector of the bias node, and WI_{bias}, WO_{bias} are the weight coefficients of the bias node 1 to the hidden layer and the bias node 2 to the output layer, respectively.

The air flow, hydrogen flow, and water flow are regarded as the input variables for the neural network model, and the generation voltage, fuel utilization and steam to carbon ratio of the MCFC system are the output variables for the ANN model. The hidden layer includes seven neurons; 8,111 data points are used to train the ANN and 4320 data points are used in the validation of the trained ANN model. Fig. 6 shows estimation results of target variables (voltage (a), fuel utilization (b) and steam to carbon ratio (c)) obtained from the ANN model. We can see that ANN model shows similar estimation performance with ARMA and LS-SVM model.

5. Partial Least Squares (PLS)

The PLS method can be regarded as a multiple linear regression model used in the modeling of relationships between inputs and outputs involving correlations [22]. This method has been used to construct black-box models using experimental or operational data. In the PLS method, the input and output data obtained from experiments or plant operations are projected onto the feature spaces with lower dimension. Then the best relationship between the feature vectors is identified by projecting high dimensional data X and Y onto some key factors (T, U). Linear regression for the relation between these key factors is followed. The relations for the input X and output Y are represented as:

$$X = TP^T + E = \sum t_h \; p_h^T + E \quad (37)$$

$$X = UQ^T + F = \sum u_h \; q_h^T + F \quad (38)$$

The coefficient b_h connecting each block can be obtained from

$$\widehat{u_h} = b_h t_h \quad (39)$$

Usually, the least-squares method is employed to calculate the regression coefficient $b_h(=u_h^T t_h / t_h^T t_h)$. The nonlinear iterative partial least squares scheme is widely used as a computing algorithm to determine key factors. PLS can be classified into type I and type II. In type I, the inner relations among blocks are nonlinear, and in type II, both the inner and outer relations are nonlinear. The general form of the type I is given by:

$$\widehat{u_h} = f(t_h) + R \quad (40)$$

Various models according to the function f have been proposed. For example, f can take a quadratic form, or artificial neural network can be used as f. Fig. 7 shows estimation results of target variables (voltage (a), fuel utilization (b) and steam to carbon ratio (c)) obtained from the PLS model. We can see that the PLS model shows similar estimation performance with ARMA, LS-SVM and ANN models.

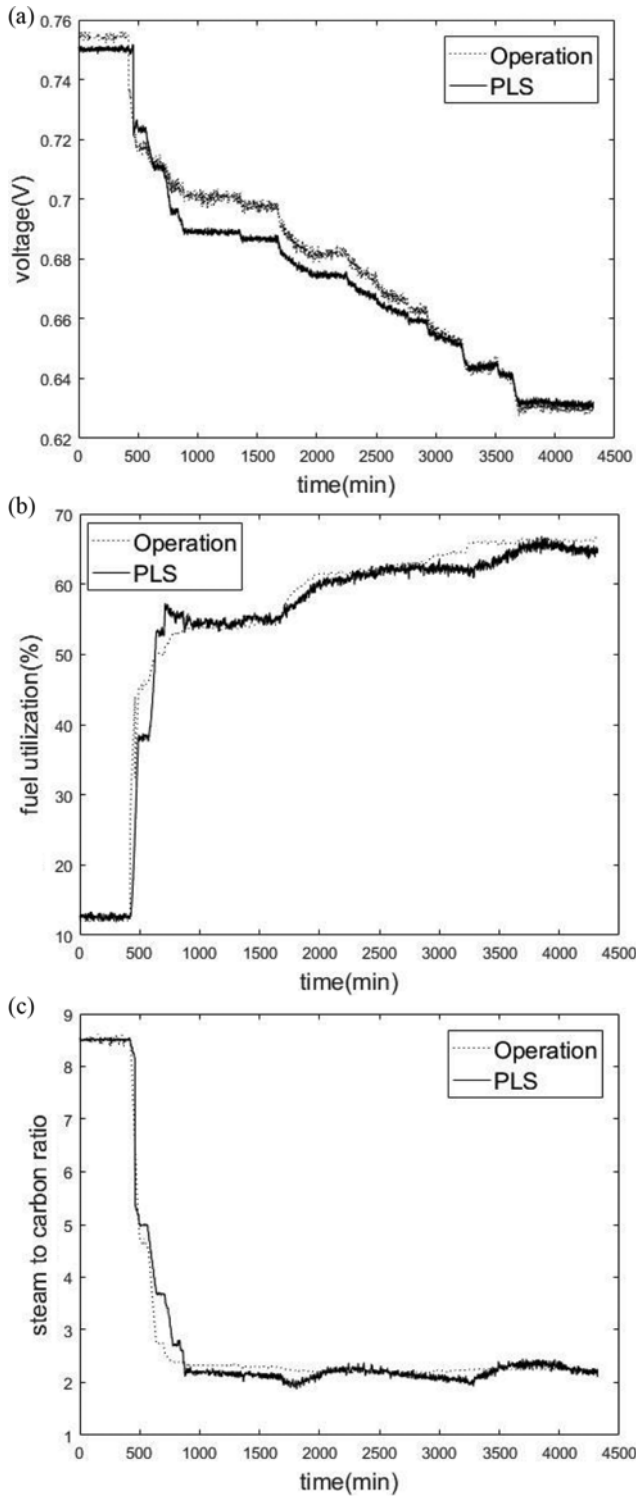

Fig. 7. Simulation results by using PLS model: (a) Voltage, (b) fuel utilization and (c) steam to carbon ratio.

MODEL COMPARISON

To compare the estimation performance of the rigorous model, the ARMA model, the LS-SVM model, the ANN model and the PLS models, values of root-mean square error (RMSE) for each model were calculated and shown in Table 2. The ARMA model exhibits the best estimation performance compared to other models. This confirms the use of the ARMA model for the analysis and design of model-based control system for the underlying MCFC plant.

Table 2. RMSE values of MCFC models

Target variable	Rigorous model	ARMA	LS-SVM	ANN	PLS
Voltage	0.0336	0.0035	0.0043	0.007	0.0068
Fuel utilization	14.73	2.71	2.87	2.81	2.73
Steam-carbon ratio	0.2401	0.1304	0.3791	0.1395	0.2459

CONCLUSIONS

To improve availability and performance of fuel cells, the output voltage of molten carbonate fuel cells (MCFC) should be controlled within a specified range. The relation of output voltage and parameters (natural gas, water, air flow) is nonlinear and complex, indicating that a nonlinear control scheme is required to adequately regulate the output voltage in case of parameter changes. In this work, various models for molten carbonate fuel cell (MCFC) processes were presented and evaluated for the purpose of identification of a comprehensive model that can be used in the model-based control of the MCFC plant. Both a rigorous model based on mass and energy balances and implicit models based on operation data were analyzed to assess their tracking performance. As implicit models, models based on auto-regressive moving average (ARMA), least-squares support vector machine (LS-SVM), artificial neural network (ANN), and partial least-squares (PLS) techniques were analyzed. Among these models, the ARMA model exhibited the best tracking performance even with severe situations involving frequent grade changes. This fact suggests that the ARMA model, if updated online, is the most promising candidate in the design of a model-based control configuration for MCFC plants.

NOMENCLATURE

A : area of the cell [cm^2]
c_i : related to electrodes and electrolytes
$\tilde{C}_t$: total molar concentration [mol/m^3]
$C_{p,i}$: specific heat of i^{th} fuel or air gas entering the system [kJ/kg K]
$\overline{C}_{ps}$: specific heat of fuel cell materials excluding gases [kJ/kg K]
C_{total} : total cell number
E_A : activation energy [kJ/mol]
E_0 : cell standard potential [V]
F : faraday coefficient [J/mol V]
$H_{2,consumed}$: rate of consumption of hydrogen in the electrochemical [mol/s]
$H_{2,in}$: molar flowrate of hydrogen in the fuel cell [mol/s]
$\Delta\hat{H}_r^o$: enthalpy of total reaction of equation [kJ/mol]
I : system current [A]
J : current density [A/cm^2]

k_s : rate constants for reforming reaction
k_w : rate constants for water gas shift reaction
K_w : equilibrium constant for water gas shift reaction
m_s : mass of fuel cell materials excluding gases [kg]
$\dot{n}_l^{in}$: inlet molar flow rate of i [mol/s]
$\dot{n}_l^{out}$: outlet molar flow rate of i [mol/s]
$\dot{n}_{H_2}^{r}$: reactive molar flow rate of H_2 [mol/s]
N^{in} : total molar flow into volume V [mol/s]
N_a^{in} : inlet molar flow in anode [mol/s]
N_c^{in} : inlet molar flow in cathode [mol/s]
N_{ru}^{in} : RU inlet total molar flow [mol/s]
N_a^{out} : outlet molar flow in anode [mol/s]
N_c^{out} : outlet molar flow in cathode [mol/s]
P : total gas pressure [kg/m s^2]
P_a : pressure in anode [kg/m s^2]
P_c : pressure in cathode [kg/m s^2]
P_{CH_4} : partial pressure of CH_4 [kg/m s^2]
P_{CO} : partial pressure of CO [kg/m s^2]
P_{H_2} : partial pressure of H_2 [kg/m s^2]
P_{H_2O} : partial pressure of H_2O [kg/m s^2]
$P_{CO_2,a}$: partial pressure of C_2O in anode [kg/m s^2]
r_0 : internal resistance [Ω cm^2]
r_j : rate of reaction j [mol/L s]
r_s : rate of reforming reaction [mol/L s]
r_w : rate of water gas shift reaction [mol/L s]
R : universal gas constant [J/mol K]
R_i : total production rate of species [mol/s]
s/c ratio : steam to carbon ratio
T_0 : ambient temperature [K]
T_{in} : inlet temperature [K]
T_{ref} : reference temperature [K]
T_s : stack temperature [K]
U_f : fuel utilization
V : compartment volume [m^3]
V_0 : equilibrium cell potential [V]
V_a : anode compartment volumes [m^3]
V_c : cathode compartment volumes volume [m^3]
V_{cell} : stack voltage [V]
x_i : mole fraction of gas species i
x_i^{in} : inlet mole fraction of gas species i
$x_{ru,\,CH_4}^{in}$: RU inlet gas mole fractions of CH_4
$x_{ru,\,CO}^{in}$: RU inlet gas mole fractions of CO
$x_{ru,\,H_2}^{in}$: RU inlet gas mole fractions of H_2
x_i^{out} : outlet mole fraction of gas species i
z : cell ohmic impedance [Ω cm^2]
η_{act} : activation polarization [V]
η_{conc} : concentration polarization [V]
v_{ij} : stoichiometric coefficients of species i in reaction j

REFERENCES

1. W. He, *J. Power Sources*, **52**, 179 (1994).
2. W. He, *J. Power Sources*, **55**, 25 (1995).
3. J. B. Ernest, H. Ghezel-Ayagh and A. K. Kush, Proceedings of the 1996 fuel cell seminar, Orlando, FL, U.S.A., 75 (1996).
4. M. D. Lukas, K. Y. Lee and H. Ghezel-Ayagh, *IEEE Trans. Energy Conver.*, **14**(4), 1651 (1999).
5. Z. Li, W. Zhong, Y. Liu, N. Luo and F. Qian, *Korean J. Chem. Eng.*, **32**(4), 597 (2015).
6. M. Sheng, M. Mangold and A. Kienle, *J. Power Sources*, **162**, 1213 (2006).
7. C. Shen, G.-Y. Cao and X.-J. Zhu, *Simulation Modeling Practice and Theory*, **10**, 109 (2002).
8. C. Shen, G.-Y. Cao, X.-J. Zhu and X.-J. Sun, *J. Process Control*, **12**, 831 (2002).
9. F. Ahmed, H. J. Cho, J. K. Kim and Y. K. Yeo, *Korean J. Chem. Eng.*, **32**(6), 1029 (2015).
10. M. Farooque, H. C. Maru and B. Baker, Proceedings of the 28th intersociety energy conversion engineering conference, Atlanta, GA, U.S.A., 181 (1993).
11. M. D. Lukas, K. Y. Lee and H. Ghezel-Ayagh, *Control Engineering Practice*, 197 (2002).
12. M. D. Lukas, K. Y. Lee and H. Ghezel-Ayagh, Proceedings of the 2000 IEEE power engineering society summer meeting, Seattle, WA, U.S.A., 1793 (2000).
13. M. D. Lukas and K. Y. Lee, *Fuel Cells*, **5**(1), 115 (2005).
14. AKM M. Murshed, Biao Huang and K. Nandakumar, *J. Power Sources*, **163**, 830 (2007).
15. J. H. Hirschenhofer, D. B. Stauffer, R. R. Engleman and M. G. Klett, Fuel cell handbook, US, Department of Energy (1998).
16. S. E. Said, D. David and A. Dickey, *Biometrika*, **71**(3), 599 (1984).
17. J. A. K. Suykens, *Proceeding of IEEE Instrumentation and measurement technology*, Budapest, 287 (2001).
18. P. Samui, *Scientific Research*, 431 (2011).
19. H. Wang and D. Hu, *IEEE*, 279 (2005).
20. M. T. Hagan, H. B. Demuth and M. H. Beale, Boston, MA: PWS Publishing Company (1996).
21. Y. D. Tian, X. J. Zhu and G. Y. Cao, *J. University of Science and Technology Beijing*, **12**, 72 (2005).
22. D. M. Haaland and E. V. Thomas, *Anal. Chem.*, **60**(11), 1193 (1988).